

SHALLOW-WATER FLOW AROUND MODEL CONICAL ISLANDS OF SMALL SIDE SLOPE. I: SURFACE PIERCING

By Peter M. Lloyd¹ and Peter K. Stansby²

ABSTRACT: A series of experiments has been conducted to investigate recirculating shallow-water flow in the wakes of conical model islands with gently sloping sides. Four islands have been used with side slopes ranging from 33.1 to 8.0°. For all tests reported here the water depth was less than the island height; the islands are said to be surface piercing. Measurements of flow velocity have been made in the laboratory using a digital particle tracking velocimetry (PTV) system. This produces instantaneous, whole-field velocity vector maps of the wake flows. A "wake stability parameter," S has been used to classify the island wakes into "vortex shedding" or "unsteady bubble" types. The stability parameter is a measure of the stabilizing effect of bed friction relative to the destabilizing influence of transverse shear. For small values of S (<0.2) vortex shedding was well organized and vigorous in the island wakes. Vortex shedding was found to cease for larger values of S (0.35–0.40). These values are similar to those found by other researchers for the shallow wakes of vertically sided circular cylinders. The influence of the island side slope angle on the wakes is discussed. Depth-averaged and three-dimensional (3D) numerical shallow-water flow models with the usual hydrostatic pressure assumption have been used to simulate the experimental flows. The models are based on a fully coupled semi-implicit Lagrangian numerical method. For cases where vortex shedding occurred, the 3D model was found to predict a more 3D far wake than was observed. The two-dimensional (2D) model produced good overall agreement with experimental results. For very shallow depths with the wake stabilized by bed friction, the 3D model demonstrated closer agreement to the measured results than the 2D model.

INTRODUCTION

In coastal and estuarial regions large-scale eddies can occur because of separation-like effects caused by flow past a headland, promontory, breakwater, or island. Such eddies are of considerable concern in a range of environmental engineering problems because of the significant influence they can exert on solute and sediment trapping. The following are specific examples of environmental concern: (1) Dilution rates for sewage, industrial effluents, and heat or radioactive discharges into coastal waters (Falconer 1993); (2) sediment transport fluxes and erosion and deposition rates in the lee of headlands, islands, and coastal basins; and (3) the long-term implications for marine fauna as well as for the location of commercial fisheries and fish farms (Hartnett 1993). Examples of air-photo and satellite images of such flows have been published by Pattiaratchi et al. (1986) and Wolanski (1986), where increased quantities of suspended material in the recirculating flow regions acted as a passive tracer.

The flow structure within a shallow-water wake flow, for which the depth of flow is an order of magnitude or more smaller than a typical horizontal length scale (e.g., the width of the wake), is very different from that with deep water. It is well documented that in a deep uniform flow incident on a two-dimensional (2D) cylinder with its axis vertical, vortex shedding occurs with strong three-dimensional (3D) components (Berger and Wille 1972). The spanwise length scale of vortices is roughly proportional to the width of the wake. The confinement, which occurs between the bed and free surface in shallow-water wakes, results in the following two important distinguishing characteristics relative to the deepwater case, namely: (1) Flow structures with two distinct length scales are

produced; large-scale recirculation zones, with a horizontal length scale comparable with the wake width and small-scale turbulence generated by bed friction, with a length scale of the order of the water depth; and (2) as a result of the confinement imposed by the shallow-water depth the large-scale recirculation zones tend to be 2D in character.

Quantitative studies on the stabilizing influence of bed friction on shallow flows with transverse shear have been made by Chu et al. (1983). They performed a linear, inviscid stability analysis on a shear layer idealized as a parallel shear flow with a hyperbolic-tangent velocity profile and the influence of bed friction added. From their analysis Chu et al. introduced a "bed-friction parameter" describing the ratio of horizontal shear to vertical shear for such flows. Using an order of magnitude analysis Ingram and Chu (1987) manipulated the bed-friction parameter into a form suitable for application to wake flows, producing the "wake stability parameter" S , given by

$$S = \frac{c_f D}{h} \quad (1)$$

where c_f = bottom friction coefficient; D = cross-stream diameter for the body; and h = water depth. Experiments conducted by Chen and Jirka (1995) using circular cylinders and flat plates have shown that the nature of the recirculation zones in the wake is critically dependent on the value of the wake stability parameter. They suggest the existence of two critical values $S_{c1} \approx 0.20$ and $S_{c2} \approx 0.50$. When $S < S_{c1}$ eddy shedding in the manner of a Kármán vortex street wake was observed. For $S_{c1} < S < S_{c2}$ the wake underwent transition from vortex shedding to a unsteady bubble type flow with instabilities growing downstream of a recirculating bubble attached to the body and for $S > S_{c2}$ the transverse disturbances ceased and the wake was characterized by a steady wake bubble with slowly recirculating flow.

Wolanski et al. (1984) derived an alternative classification for shallow-water wakes in the form of the "island wake parameter" P , giving

$$P = \frac{Uh^2}{K_z D} \quad (2)$$

where U = ambient velocity; and K_z = a vertical eddy diffusion coefficient. The two wake parameters S and P share an inverse

¹Res. Assoc., Hydrodynamics Res. Group, The Manchester School of Engrg., Univ. of Manchester, Manchester M13 9PL, U.K.

²Prof. of Hydrodynamics, Hydrodynamics Res. Group, The Manchester School of Engrg., Univ. of Manchester, Manchester M13 9PL, U.K.

Note. Discussion open until May 1, 1998. Separate discussions should be submitted for the individual papers in this symposium. To extend the closing date one month, a written request must be filed with the ASCE Manager of Journals. The manuscript for this paper was submitted for review and possible publication on November 13, 1996. This paper is part of the *Journal of Hydraulic Engineering*, Vol. 123, No. 12, December, 1997. ©ASCE, ISSN 0733-9429/97/0012-1057-1067/\$4.00 + \$.50 per page. Paper No. 12346.

relationship where $S \sim (c_f)^{1/2}/P$. As stated by Ingram and Chu (1987), because c_f does not vary substantially from one situation to another the two methods of classification are very similar. In this paper we will use S to describe the wake characteristics, enabling direct comparison with other experimental programs that have used this parameter exclusively [e.g., Chen and Jirka (1995)].

Numerical models based on the shallow-water equations are widely used for predicting flows with recirculation in coastal and estuarial waters. However, these models embody a number of assumptions concerning the physical processes and these assumptions, with the numerical dissipation inherent in most numerical solutions, make the accuracy of results uncertain and, to some extent, problem dependent. Some problems of this kind have been demonstrated by Falconer et al. (1986), who used a depth-averaged, alternating direction implicit (ADI) finite-difference model to simulate the flow around Rat-tray Island situated off the northeast Australian coast. The representation of lateral shear stresses, advective acceleration terms, and the accuracy of the island bathymetry specification were all found to have a significant influence.

In this paper a series of laboratory experiments has been conducted to investigate the shallow-water wakes of conical model islands of small slope. The results presented here concern cases for which the water depth is less than the height of the island and the flow is subcritical. A related series of experiments on the wakes of submerged islands will be presented in Part II. The conical models represent a closer approximation of natural depth-varying bathymetries than vertical sided models. A range of side slope angle has been used to assess the effect on the wake flow. Measurements of velocities in the laboratory have been made using a particle tracking velocimetry (PTV) system, which produces instantaneous whole-field surface velocity vector maps. Such velocity maps provide information on the evolution, transport, and relative scales of eddy structures within the flow and are recognized as being useful for computational model validation studies [e.g., Wu and Tsanis (1994)].

The experimental setup provides simple boundary conditions for collecting benchmark data for comparison with numerical model results. The depth-varying bathymetry of the islands and the unsteady nature of the wake flow provide a challenging problem to model accurately. In this paper we use depth-averaged 2D and 3D numerical models of the shallow-water equations to simulate the experimental flows. The models are formulated using a semi-implicit Lagrangian finite-difference scheme with the usual hydrostatic pressure assumption. Such comparisons are valuable in assessing how assumptions made in the models affect the quality of the simulation and provide an interesting basis for contrasting the 2D and 3D schemes.

EXPERIMENTAL ARRANGEMENT

The experiments were conducted in a shallow-water flume situated in the hydrodynamic laboratory at Manchester University. The flume, illustrated schematically in Fig. 1, has horizontal dimensions of 9.75 by 1.52 m. The bed and sidewalls were constructed from marine quality plywood, except for a central region where transparent Perspex viewing panels replaced the wooden walls. An arrangement of wire mesh, a polyvinyl chloride (PVC) baffle, and 10 aluminium flow straighteners (see Fig. 1) helped to produce transverse velocity profiles with a variation within $\pm 7\%$ of the mean.

The free-stream flow is described by the depth Reynolds number R_h , given by

$$R_h = \frac{U_0 h}{\nu} \quad (3)$$

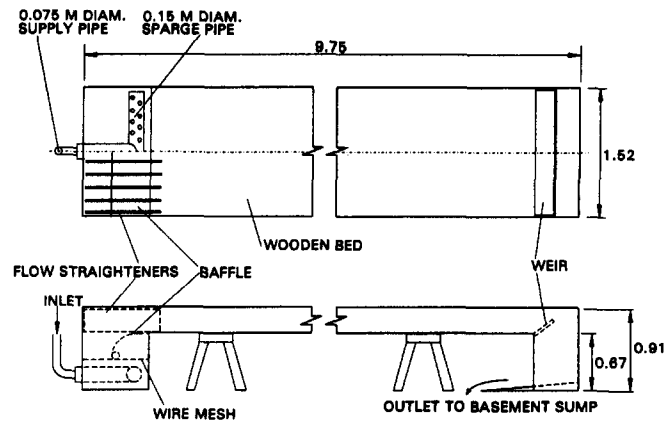


FIG. 1. 1.52-m-Wide-Shallow-Water Flume in Hydrodynamics Laboratory at Manchester University

where U_0 = mean free-stream velocity, measured using a propeller meter and checked by timing the movement of floating particles over a fixed distance; h = water depth; and ν = kinematic viscosity. For the series of surface-piercing tests described here the mean flow was a fully developed turbulent free stream, with R_h ranging between 1,300 and 7,040 and the Froude number $U_0/(gh)^{1/2}$ always less than 0.3. The influence of roughness in a turbulent boundary layer in an open channel flow may be classified by the Reynolds number R_* based on the bed roughness height k_s and the friction velocity u_* [e.g., French (1994)] where

$$R_* = \frac{u_* k_s}{\nu} \quad (4)$$

According to this classification, flows in the test series described here were in the smooth turbulent regime. A Reynolds number based on a representative body dimension is defined as

$$R_d = \frac{U_0 D_a}{\nu} \quad (5)$$

where D_a = island diameter at the middepth.

The bed-friction coefficient c_f is evaluated using the smooth pipe formula, with the pipe diameter replaced for four times the water depth as recommended by Carter et al. (1963)

$$\frac{1}{\sqrt{c_f}} = -4 \log \left(\frac{1.25}{4R_h \sqrt{c_f}} \right) \quad (6)$$

The wake stability parameter, discussed in the preceding section, is calculated for the conical models using the diameter at middepth as the cross-stream dimension, giving

$$S = \frac{c_f D_a}{h} \quad (7)$$

A summary of experimental test conditions for which detailed measurements were collected is presented in Table 1.

Four aluminium model islands have been used with dimensions (in meters) given in Fig. 2. Where θ is side slope angle, "island 1" will denote the model with $\theta = 33.1^\circ$, "island 2" with $\theta = 22.2^\circ$, "island 3" with $\theta = 12.6^\circ$, and "island 4" with $\theta = 8.0^\circ$. The models were secured centrally in the flume at a position 5.0 m downstream of the inlet where the flow was fully developed. The same paint used on the flume bed was used for the models producing a similar surface roughness. The base diameter of island 4 is half the width of the flume and it is possible that the limited channel width could influence the results. However, numerical tests with a flume width of 3.0 m produced results that were almost identical to those produced with a 1.5-m-wide flume.

TABLE 1. Summary of Experimental Conditions for Surface-Piercing Island Study

Model number (1)	Run (2)	U_0 (m/s) (3)	h (m) (4)	D_s (m) (5)	R_b (6)	R_d (7)	c_f (8)	S (9)
2	SP2.01	0.088	0.0800	0.334	7,039	29,389	0.005953	0.0249
3	SP3.01	0.115	0.0510	0.411	5,865	47,296	0.006219	0.0501
3	SP3.02	0.115	0.0420	0.452	4,830	51,938	0.006520	0.0701
3	SP3.03	0.115	0.0220	0.541	2,530	62,253	0.007688	0.1892
3	SP3.04	0.100	0.0185	0.557	1,850	55,703	0.008364	0.2518
3	SP3.05	0.100	0.0160	0.568	1,600	56,824	0.008707	0.3092
3	SP3.06	0.100	0.0150	0.573	1,500	57,272	0.008866	0.3385
3	SP3.07	0.100	0.0140	0.577	1,400	57,721	0.009040	0.3727
3	SP3.08	0.100	0.0135	0.579	1,350	57,945	0.009134	0.3921
3	SP3.09	0.100	0.0130	0.582	1,300	58,169	0.009233	0.4131
4	SP4.01	0.115	0.0450	0.429	5,175	49,287	0.006410	0.0611
4	SP4.02	0.115	0.0350	0.500	4,025	57,501	0.006822	0.0975
4	SP4.03	0.115	0.0260	0.564	2,990	64,893	0.007359	0.1597
4	SP4.04	0.100	0.0190	0.614	1,900	61,429	0.008303	0.2685
4	SP4.05	0.100	0.0175	0.625	1,750	62,500	0.008493	0.3033
4	SP4.06	0.100	0.0160	0.636	1,600	63,571	0.008707	0.3459
4	SP4.07	0.100	0.0150	0.643	1,500	64,286	0.008866	0.3800
4	SP4.08	0.100	0.0145	0.646	1,450	64,643	0.008951	0.3990

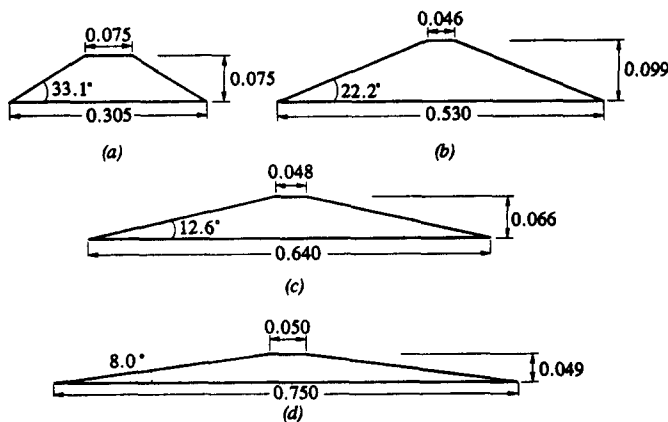


FIG. 2. Conical Model Island Geometries: (a) Island 1, $\theta = 33.1^\circ$; (b) Island 2, $\theta = 22.2^\circ$; (c) Island 3, $\theta = 12.6^\circ$; (d) Island 4, $\theta = 8.0^\circ$

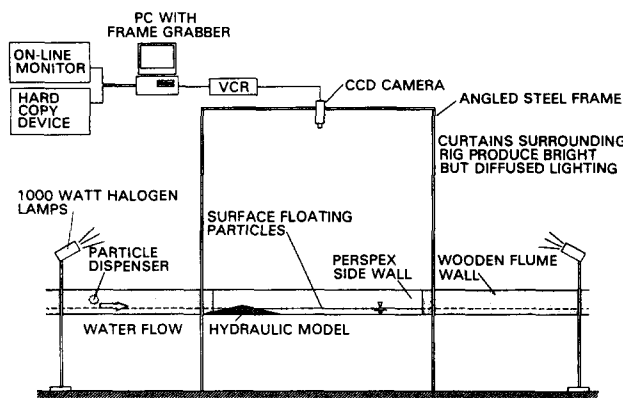


FIG. 3. Schematic View of PTV Setup

The PTV system has been designed to measure velocities over relatively large test sections and is thus well suited to hydraulic model studies in the laboratory (Lloyd et al. 1995). Fig. 3 provides a schematic view of the test setup. The test section is illuminated and several hundred 5-mm-diameter solid black polypropylene beads are released onto the water surface to act as tracer particles. The particles float at the free surface (almost submerged), allowing water-surface velocities to be measured. The particles in the flow are filmed from above with a charge coupled device CCD camera and recorded on video tape. A test section of 1.5×1.3 m is provided by

the camera and lens arrangement. The video recorder is connected to a personal computer (PC) fitted with a digital frame grabber card. Using the frame grabber, two frames of the video recording are digitized (an image pair) with a short time separation (≈ 0.24 s). A program has been written in Fortran 77 to analyze the image pair and produce velocity vectors from the seeding particle movement. Individual particles are tracked, which leaves velocity vectors in an unstructured distribution across the image plane and an interpolation routine is used to regularize the vector field.

The accuracy of the PTV velocity measurements has been assessed by comparison with simultaneous laser Doppler anemometer (LDA) measurements in the wake of island 2. With $U_0 = 0.088$ m/s and $h = 0.080$ m, the average PTV error was measured to be less than 10%.

COMPUTATIONAL MODELS

Two numerical models have been used for comparison with the experimental test series. The depth-averaged 2D model uses a finite-difference formulation for the shallow-water equations based on the semi-implicit Lagrangian scheme of Casulli (1990). In the Lagrangian description of the advective terms the total derivative for velocity is used. Upwind differencing is thus avoided with the method proving stable, less numerically diffusive, and, although explicit, unrestricted by the Courant condition. A semi-implicit form of the Manning formula was used in the code available to represent the components of bed-shear stress, with Manning's roughness coefficient n set to 0.01 s/m^{1/3}. Although Manning's formula strictly assumes rough turbulent conditions, appropriate values may be obtained by linking depth, flow velocity, and bed slope in normal conditions.

A 3D model of the shallow-water equations is developed from the formulation of Casulli and Cheng (1992). The hydrostatic pressure assumption implies that the horizontal pressure gradients are independent of vertical position. The physical implication is that weak or secondary effects driven by attached boundary layers in the vertical direction are reproduced whereas gross effects such as flow separation or steep wave evolution are not. The σ -coordinate system for the vertical direction enables the vertical velocity gradients to be computed accurately, which is particularly important at the bed and free surface where shear stress boundary conditions are imposed; the logarithmic law of the wall for the former and zero shear stress for the latter.

For both models an eddy viscosity μ_H for horizontal mixing

was defined locally as $\mu_H = \rho c_H u_* h$, where ρ is the fluid density and c_H is a mixing coefficient. The c_H is set here to 0.10 although increasing or decreasing this value by an order of magnitude was found to have little effect on the results produced. A standard two-layer mixing-length model for eddy viscosity was used to describe vertical mixing in the 3D model. A detailed account of model formulation and testing may be found in Stansby and Lloyd (1995).

RESULTS

Experimental Measurements and Observations

Experimental runs were performed with the value of the wake stability parameter below 0.10 to investigate the model island wakes with a relatively small bed friction influence. For quantitative studies using PTV, model island 2 ($\theta = 22.2^\circ$), island 3 ($\theta = 12.6^\circ$), and island 4 ($\theta = 8.0^\circ$) were used (see Table 1) with the ratio of water depth to island height h/h_i always greater than 0.7. Some qualitative flow visualization experiments were conducted using island 1 (not listed in Table 1).

The model islands produced wakes that were broadly similar in appearance, characterized by vigorous, periodic vortex shedding. For such small values of S , the wakes observed in the laboratory appeared qualitatively similar to the Kármán vortex sheet observed behind a circular cylinder (with minimal end effects) in the Re range of 100–300 [see Gerrard (1978)]. The values of the Reynolds number based on the island diameter in the present experiments were of $O(10^4)$. A similar observation was made by Chen and Jirka (1995) for the shallow wake flows of circular cylinders. They noted that because of the limited vertical dimension, which prevents vortex breakdown, well organized eddy systems remained visible for much larger values of Re than traditionally found in wakes of long cylinders. Fig. 4(a) presents an instantaneous surface velocity vector field, measured using the PTV system, of a typical vortex shedding wake. The plot clearly illustrates the recirculating, oscillatory nature of the flow field. The case illustrated is test number SP2_01 with island 2 ($\theta = 22.2^\circ$). For this case the mean velocity $U_0 = 0.088$ m/s and the water depth $h = 0.08$ m, with the wake stability parameter $S = 0.025$. The structure of the flow is further illustrated in Fig. 4(b), which shows a contour plot of the z -component of surface vorticity ($\omega = \partial v/\partial x - \partial u/\partial y$) for the velocity plot of Fig. 4(a) (nondimensional $\omega^* = \omega D_i/U_0$). Values of vorticity are calculated using a finite-difference approximation from the velocity vector fields interpolated on to a regular mesh. Evidence of near-wake interaction between the horizontal shear layers formed from the flow around the island sides can be seen from the patch of positive vorticity directly downstream of the island about to be entrained into the negative patch about to be shed. Such interaction is also an integral part of the vortex shedding mechanism for long cylinders (Gerrard 1966).

To examine the effect of increasing bed friction on the model island wakes, experiments were conducted in a range of the wake stability parameter S identified by previous studies as classifying transition from a vortex street to an unsteady bubble wake (for the flow about a circular cylinder). As the depth of the flow in these experiments decreases, both the magnitude of the bed-friction coefficient c_f and the effective diameter of the island D_e increase. Lowering the flow depth thus acts to increase significantly the magnitude of the wake stability parameter S .

The results of dye visualization tests are illustrated in Figs. 5(a–d). Digital images of the wake of model island 4 ($\theta = 8.0^\circ$) are shown as the wake stability parameter is increased from $S = 0.06$ to $S = 0.40$. Methylene blue dye was released upstream of the island and the images were produced once the

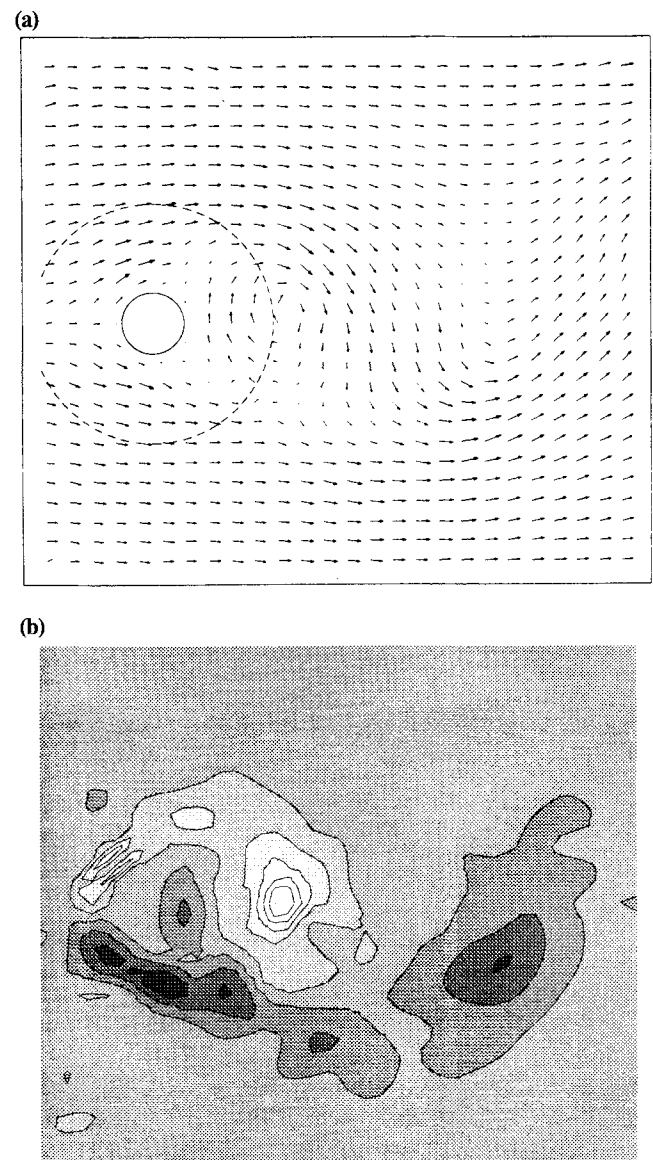


FIG. 4. Experimental Flow around Island 2: (a) Surface Velocity Vector Field; (b) Surface Vorticity Field

recirculating wake zone had become saturated. Figs. 6(a–d) show surface velocity vector plots produced by the PTV system for the wakes illustrated in Figs. 5(a–d). Note that the velocity fields are not necessarily produced at the same time in the eddy cycle as the images shown in Fig. 5.

Figs. 5(a) and 6(a) show the wake of test case SP4_01, with $S = 0.06$, to consist of vigorous well organized vortex shedding. Figs. 5(b) and 6(b) show test SP4_04 with S increased to 0.270. Regular vortex shedding is still occurring, although the rolled-up vortex contains lower velocities relative to the previous case. With S increased to 0.35, shown in Figs. 5(c) and 6(c) for case SP4_06, the size of the rolled-up vortex has increased and the apparent origin of vortex shedding has moved further downstream. Velocities in the near-wake region are low (with a maximum of approximately $0.35-0.4U_0$) and the interaction between the horizontal shear layers is weak. The wake of test case SP4_08, with $S = 0.40$, is presented in Figs. 5(d) and 6(d). Any form of well-organized vortex shedding has ceased to exist with the wake now appearing as an “unsteady bubble” flow. This consisted of a bubble region with two zones of opposite recirculation attached to the island and low-frequency transverse oscillations downstream. Measurements in the flume indicated flow returning along the wake centerline from a distance of up to 1.75 m downstream of the

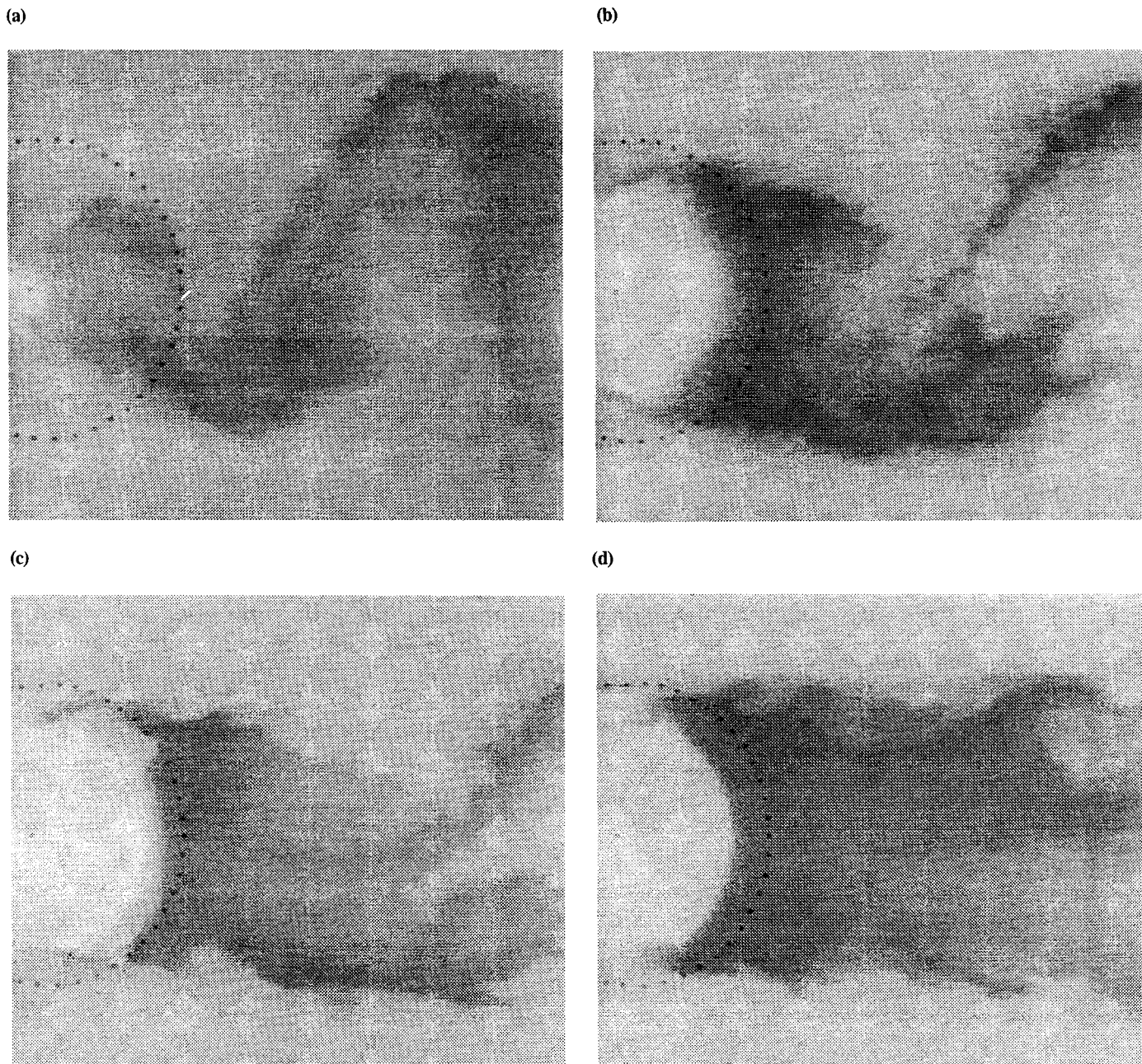


FIG. 5. Dye Visualization of Wake of Island 4 ($\theta = 8.0^\circ$): (a) $S = 0.06$; (b) $S = 0.27$; (c) $S = 0.35$; (d) $S = 0.40$

island center (outside the area shown in the figures). The maximum velocity of the return flow was approximately $0.3U_0$.

Estimates of flushing times T_f were made for the wakes shown in Figs. 5(a–d) by recording the time taken for the dye-saturated wake to clear. Measurements were started when a fixed quantity of dye had been released from a supplying reservoir. The wake was defined as “clear” when the digital image pixel gray levels of the near-field region returned to their original values. Although only approximate, the results support the findings of Chen and Jirka (1991) who found dye to take up to 11 times longer to flush from an unsteady bubble-type wake with $S = 0.36$, compared with a vortex shedding wake with $S = 0.15$. The T_f for the wake shown in Fig. 5(d) with $S = 0.40$ was approximately nine times larger than for the vigorous eddy system illustrated in Fig. 5(a) ($S = 0.06$). With S calculated at 0.27, T_f was approximately twice as large as that for $S = 0.06$ and three times when $S = 0.35$.

Similar results were obtained when model island 3 ($\theta = 12.6^\circ$) was tested, with the transition from vortex shedding to

an unsteady bubble wake occurring for a value of S between 0.35 and 0.40.

The observed results, with vortex shedding suppressed by bed friction for $S > 0.35$, are consistent with the work of other researchers. From the results of open channel flow experiments containing steady recirculation zones, Babarutsi et al. (1989) suggested vortex shedding would cease in the wake of an island for $S \approx 0.40$. The value of the wake stability parameter, which marks the transition from vortex shedding to a recirculating bubble wake in this study, is toward the middle of the range proposed by Chen and Jirka (1995) ($S = 0.20$ – 0.50) for circular cylinders. However, with experiments involving conical islands there is some arbitrariness about the choice of model diameter when calculating S . The diameter of a conical model at the middepth D_a was felt to be a reasonable representation of model size. There is also some uncertainty in defining the boundary S value between an unsteady bubble wake and a vortex shedding wake. A wake flow does not jump from one type to another; the boundary is fuzzy.

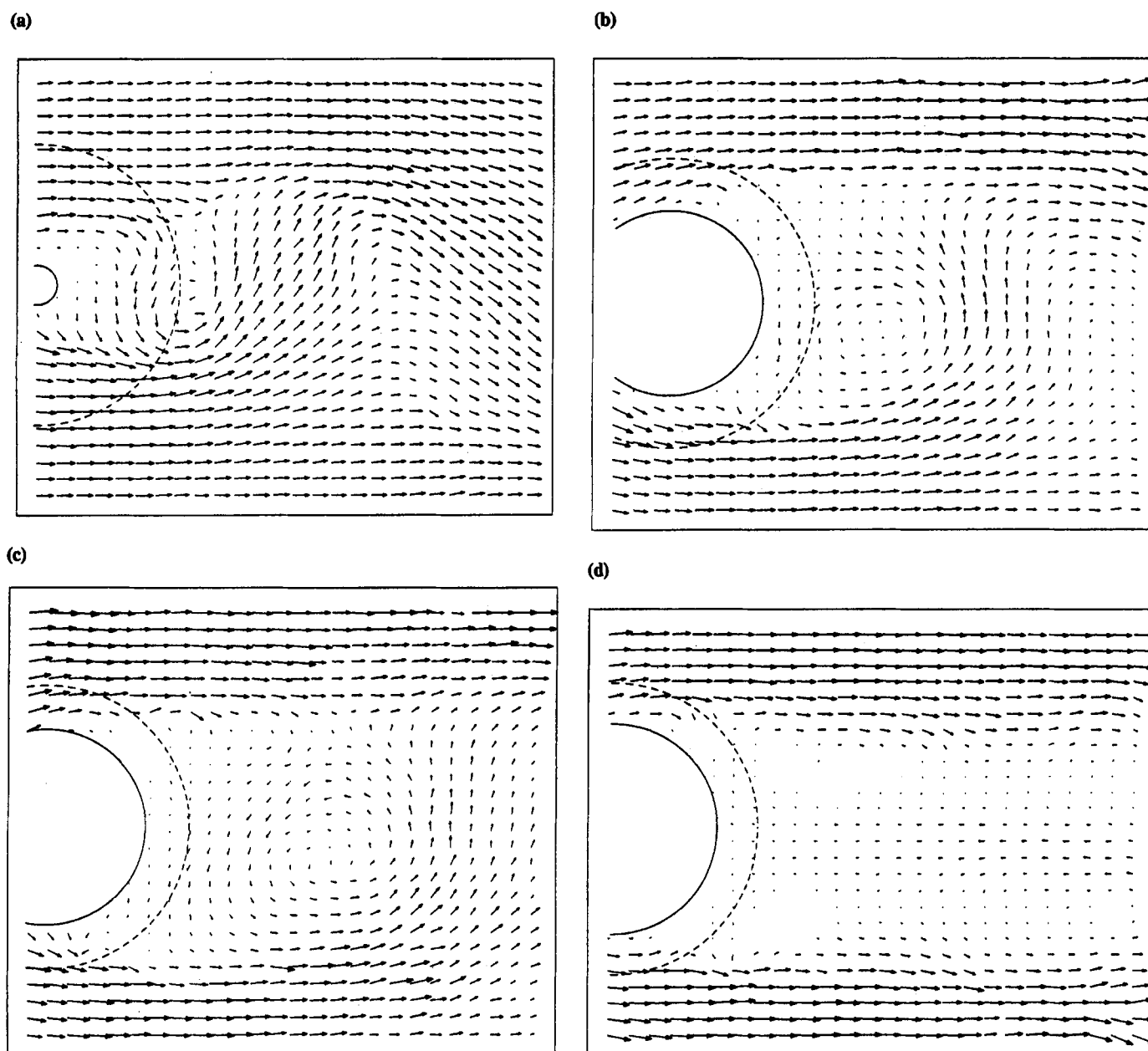


FIG. 6. Experimental Surface Velocity Vector Fields of Wake of Island 4 ($\theta = 8.0^\circ$): (a) $S = 0.06$; (b) $S = 0.27$; (c) $S = 0.35$; (d) $S = 0.40$

The horizontal shear layers forming at either side of the island and the recirculating near-wake zone are complex turbulent regions that govern the formation of the far-field wake downstream. The surface PTV measurements described the large-scale turbulent structures present in the flow but shed little light on the formation of such vortices or the flow characteristics across the depth. Dye visualization tests, using both methylene blue and potassium permanganate crystals (KMnO_4), were performed with the aim of depicting any interesting small-scale features. A sketch of some of these features is presented in Fig. 7.

In the near wake there is a region of very low velocity. Horizontal shear layers are produced between this region and the accelerated flow around the island. For small values of the wake stability parameter it is these layers that interact to produce the large-scale vortices in the far field. Lines of separation, delineated on the bed of the model by the KMnO_4 tracers, are drawn on the sketch in Fig. 7. Toward the upper shoulder of the islands, lines of separation were clearly formed. Flow separating from this region was subject to vigorous vertical mixing. Following separation, KMnO_4 dye, which upstream of

this region had visualized the flow direction close to the bed, quickly mixed across the depth. Energetic mixing was also apparent in the near-wake region behind the island. However, this mixing became visibly weaker as S increased. When S was large enough to stabilize vortex shedding, dye injected into the return flow along the wake centerline diffused slowly. Separation lines along the middle and lower shoulder (i.e., near the base perimeter) of the island were less clearly defined with any vertical mixing concentrated at positions close to the bed. A secondary flow was produced by the separation mechanisms with dyed fluid being observed to "drift" up the island shoulders along the separation lines on the body of the island. All four model islands tested displayed these flow characteristics.

For vortex shedding wakes, flow vanes were employed to provide information on the flow direction across the depth (Lloyd 1995). Vanes were placed at several positions along the wake centerline. Each device consisted of two rigid plastic vanes, free to rotate about a thin vertical wire in a horizontal plane, one plane near the flume bed and the other a small distance below the free surface. Although the vanes did not

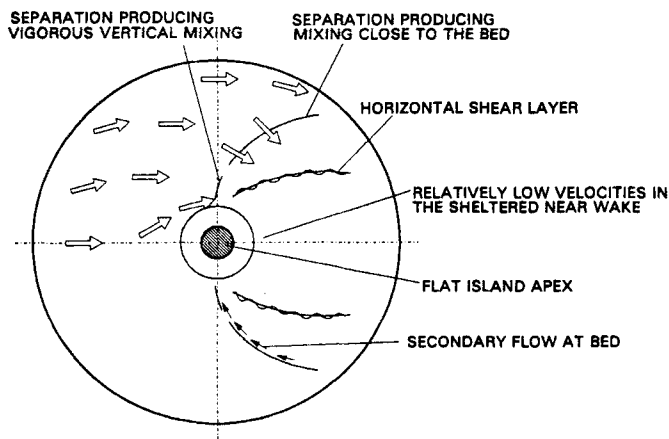


FIG. 7. Sketch of Near Wake Processes

provide velocity magnitude information, they were useful for indicating the relative phase of the unsteady flow at the two depths. Downstream of the base perimeter of the island the vanes at bed and surface moved in phase with each other, suggesting the flow to be 2D. At positions close to the island the vanes often displayed a similar dominant frequency but were not consistently in phase, indicating the existence of 3D flow components.

Model Results

The model computations in this study were made with a horizontal square cell size of 0.0152 m and a time step of 0.05 s. For all 2D runs and many of the 3D runs a 328×100 horizontal mesh was used. For some 3D simulations the downstream mesh boundary was moved upstream to save run time. The semi-implicit Lagrangian scheme was found to be insensitive to the downstream boundary conditions for the depth-averaged code (Stansby and Lloyd 1995). Reducing the length of the mesh did not significantly affect the results. The number of vertical cells in the 3D runs was set between 10 and 20. The computations reported here were made on a vector processor, the Cray EL98, with a peak processing performance of 133 Mflops. For the 2D model a run with a 328×100 mesh for 4,000 time steps required 2 h central processing unit (CPU) time, with the code vectorizing almost completely. With the same horizontal mesh size and 20 vertical divisions the 3D model required about 80 CPU hours to run 4,000 time steps. Most run times were made much shorter by reducing the number of vertical segments and/or the number of time steps.

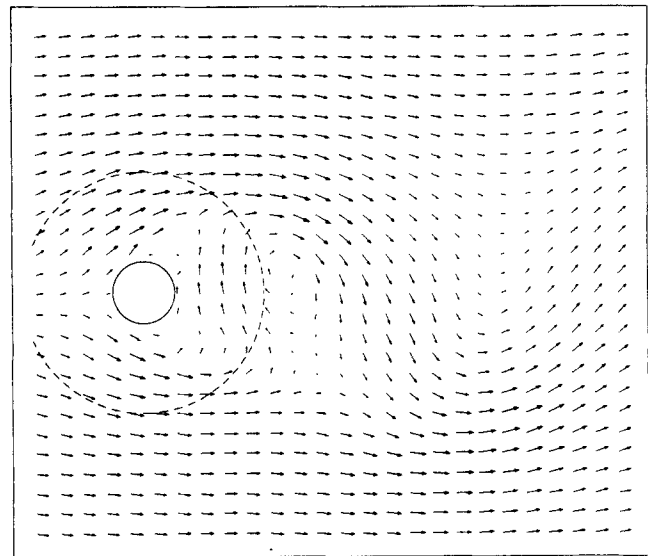
A depth-averaged velocity vector plot produced by the 2D model is presented in Fig. 8(a) for island 2 (22.2°), test number SP2_01 ($U_0 = 0.088$ m/s; $h = 0.08$ m), with the wake stability parameter $S = 0.025$. The vector field shows an area of the computational domain close to the island for comparison with the experimental PTV vector plot in Fig. 4(a). There is very good agreement between the two with the vortex size and the position of the dominant vortex center correctly predicted by the depth-averaged code. Note that the two plots are produced at a corresponding time in the vortex shedding cycle as a means of comparing the wake structure. Instantaneous vector plots produced from a time datum may not be so well matched because of differences between the model and experiment shedding frequencies. A contour plot of vorticity produced from the vector plot of Fig. 8(a) is presented in Fig. 8(b). Comparison with the corresponding experimental vorticity plot of Fig. 4(b) provides a further illustration of the model's capability for reproducing the gross flow features.

Results from the 3D model were similar. Velocity time histories of the u velocity component at a position in the far wake showed close agreement in the dominant shedding frequency

and peak-to-peak velocity magnitudes. Further details of these test results can be found in Stansby and Lloyd (1995).

The models were run to simulate the flow around the more gently sloping island 3 (12.6°), for test case SP3_01 ($U_0 = 0.115$ m/s; $h = 0.051$ m). As with the previous case the wake stability parameter was small ($S = 0.050$) resulting in a wake flow resembling a Kármán vortex street. A PTV vector plot of the surface velocities is shown in Fig. 9(a). Fig. 9(b) shows the depth-averaged velocity vectors predicted by the 2D model and Fig. 9(c) shows the velocity field at the surface cell predicted by the 3D model. Both model plots are produced across an area corresponding to the PTV measurements and at a similar time in the wake cycle. Although the 2D scheme demonstrates good qualitative agreement (at least) with experiment, the 3D scheme appears to contain a different vortex structure. In Fig. 10(a) ($\theta = 12.6^\circ$; $U_0 = 0.115$ m/s; $h = 0.051$ m), the 3D model velocity field shown in Fig. 9(c) is reproduced for the entire computational domain (a 218×100 mesh size) with the vector fields at the middepth shown in Fig. 10(b) and at the bed positions in Fig. 10(c). Differences in the wake are apparent between velocities at the free surface and mid-

(a)



(b)

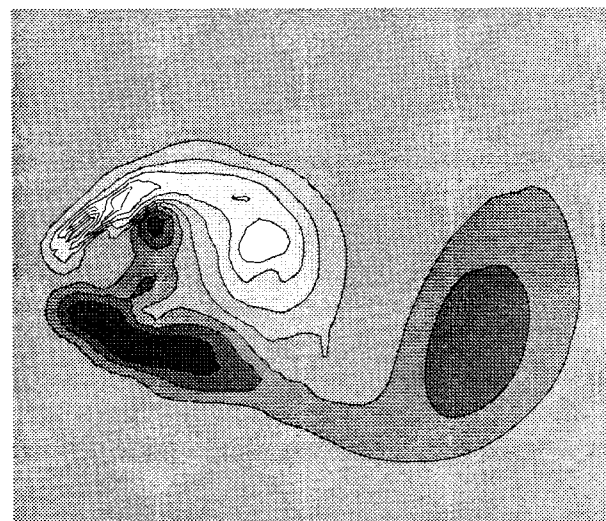


FIG. 8. 2D Model Prediction of Flow around Island 2: (a) Velocity Vector Field; (b) Vorticity Field (Nondimensional)

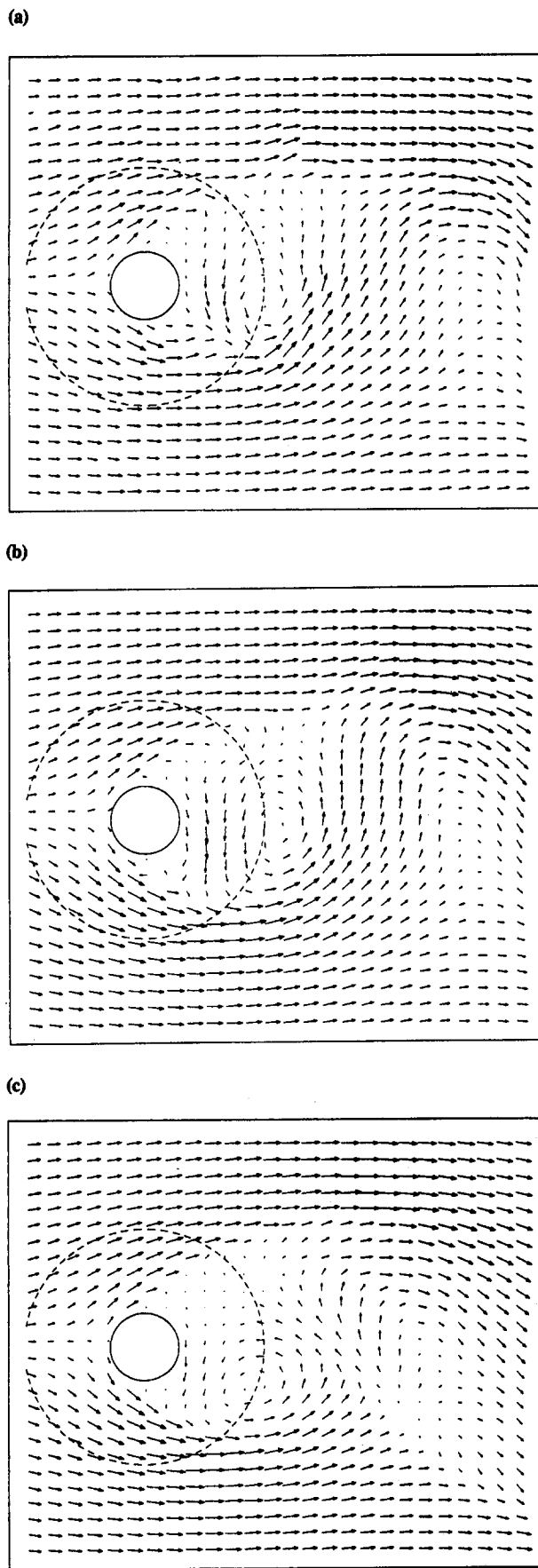


FIG. 9. Model and Experimental Velocity Vector Fields of Island 3: (a) Experimental Surface Velocities; (b) 2D Model Depth-Averaged Velocities; (c) 3D Model Surface Velocities

depth planes. Fig. 10(d) shows a 2D slice of the x, z -plane through the central y -coordinate. A vertical mixing cell is visible in the recirculating region downstream of the island's base perimeter. This may be responsible for the reorganization of the flow into a more 2D form further downstream. Comparison between velocity time histories measured experimentally with PTV and predicted by the 2D and 3D models is shown in Figs. 11(a and b), respectively ($\theta = 12.6^\circ$; $U_0 = 0.115$ m/s; $h = 0.051$ m). The measuring position is 0.73 m downstream of the island center and 0.26 m from the wake centerline. Although differences are clearly apparent between the 2D and 3D models, e.g., the structure of the u velocity traces, gross features of the wake are modeled with a similar accuracy. Both models slightly overpredict the dominant eddy shedding frequency, with mean and peak-to-peak velocity magnitudes reasonably well predicted.

The 3D model incorporates a simple two-layer mixing-

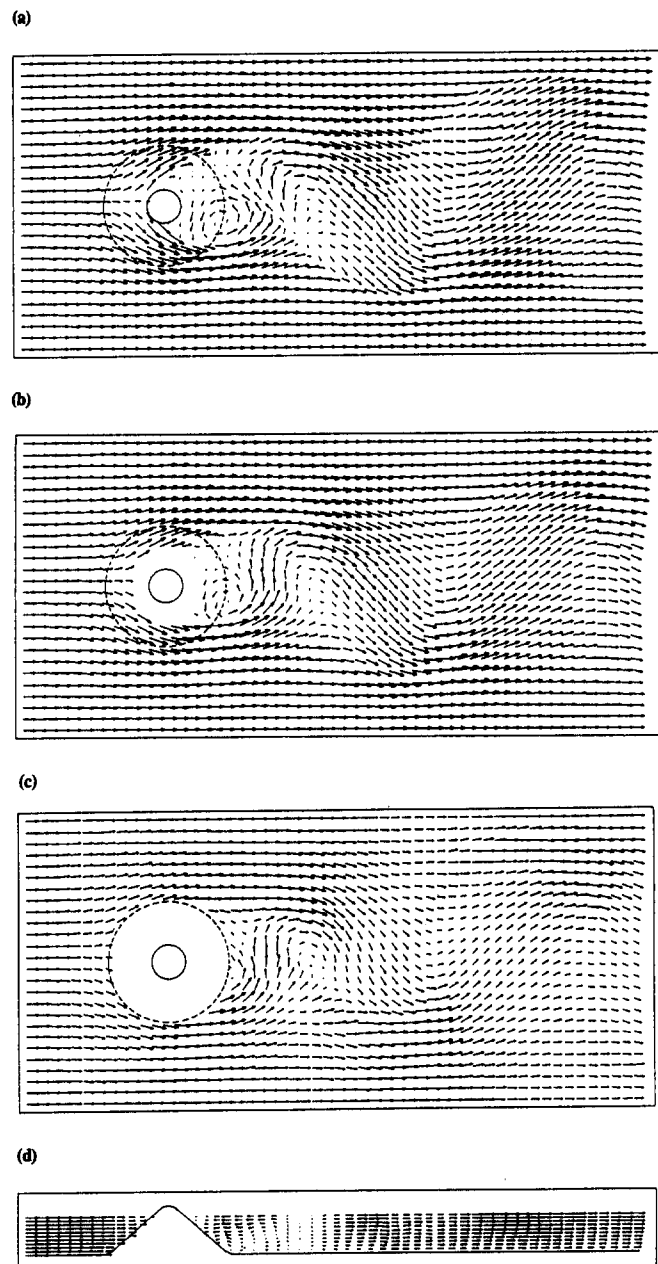


FIG. 10. Velocity Vector Field from 3D Computation of Island 3: (a) u, v , Velocities at Water Surface; (b) u, v Velocities at Mid-depth; (c) u, v Velocities at Bed; (d) u, w Velocities at Mid- y Plane with Depth Increased by a Factor of 4

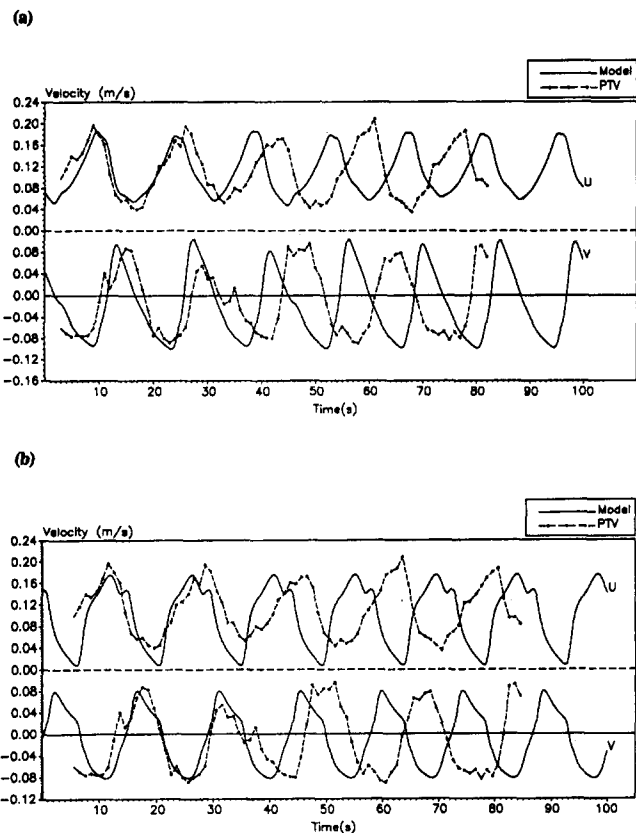


FIG. 11. Variation in Velocities u and v with Time from Experiment and Computation of Island 3: (a) 2D Model Comparison; (b) 3D Model Comparison

length turbulence model and hydrostatic pressure is assumed. Vertical accelerations are therefore neglected. The strong vertical mixing observed in the separated shear layers and the near-field wake region in the laboratory was not reproduced in the model. The relatively weak vertical mixing in the model resulted in a far wake with a greater depthwise variation in velocity than observed in the laboratory. The surface vector field plot of the well-mixed laboratory flow displayed closer resemblance to the model vector plot at the middepth plane, than to the plot at the free surface. This effect was less noticeable for the 3D run with island 2 with a greater side slope of $\theta = 22.2^\circ$. The depth-averaged model, for which mixing across the depth is, in effect, instantaneous, produced results that were in closer agreement with the PTV measurements. The effects of flow separation in a vertical plane, crucial for producing effective vertical mixing, cannot be reproduced with the hydrostatic pressure assumption. This has been demonstrated by Johns (1991), who devised a 2D vertical plane model to simulate the flow over irregular topography typical of sand dunes. The model was tested with a hydrostatic pressure assumption and then reformulated to include a contribution from nonhydrostatic pressure. With the latter model, separation was found to occur from the dune peaks, producing a recirculating cell on the lee slope. This generated turbulent energy and shear stress values approximately double those found with the hydrostatic pressure model that produced no recirculation. The nonhydrostatic pressure model produced better agreement with experimental and field measurements than the hydrostatic case (Johns et al. 1993). Development of the 2D model into a 3D nonhydrostatic pressure model is presented in Johns and Xing (1993).

The 2D and 3D shallow-water models were run for cases with larger values of the wake stability parameter S , to test

whether they could produce the stabilizing effects of bed friction on the island wakes observed in the laboratory. Note that to reduce the computational time, the 3D mesh size was reduced to $218 \times 100 \times 10$. It has already been seen how for island 4 ($\theta = 8.0^\circ$) with $S = 0.27$ [Figs. 5(b) and 6(b)], the bed friction began to alter the vortex shedding characteristics in the near wake, although a distinct oscillatory form was still present. Both the 2D and the 3D models produced reasonably good representations of this case, with the predicted shedding frequency accurate to within 5% of experiment.

Further increases in S resulted in less-accurate model simulations. This is demonstrated by the results for test case SP4.08, with S now set to 0.40, presented in Figs. 12(a and b) ($\theta = 8.0^\circ$; $U_0 = 0.100$ m/s; $h = 0.0145$ m). The velocity field predicted by the depth-averaged model shown in Fig. 12(a) bears little similarity to that observed in the laboratory. A vigorous vortex shedding structure is clearly present in the wake with strong cross-flow components in the near field. The flow field appears very similar to that predicted by the same model for $S = 0.27$. The experimental PTV vector plot for case SP4.08, shown in Fig. 6(d), consists of a steady return flow

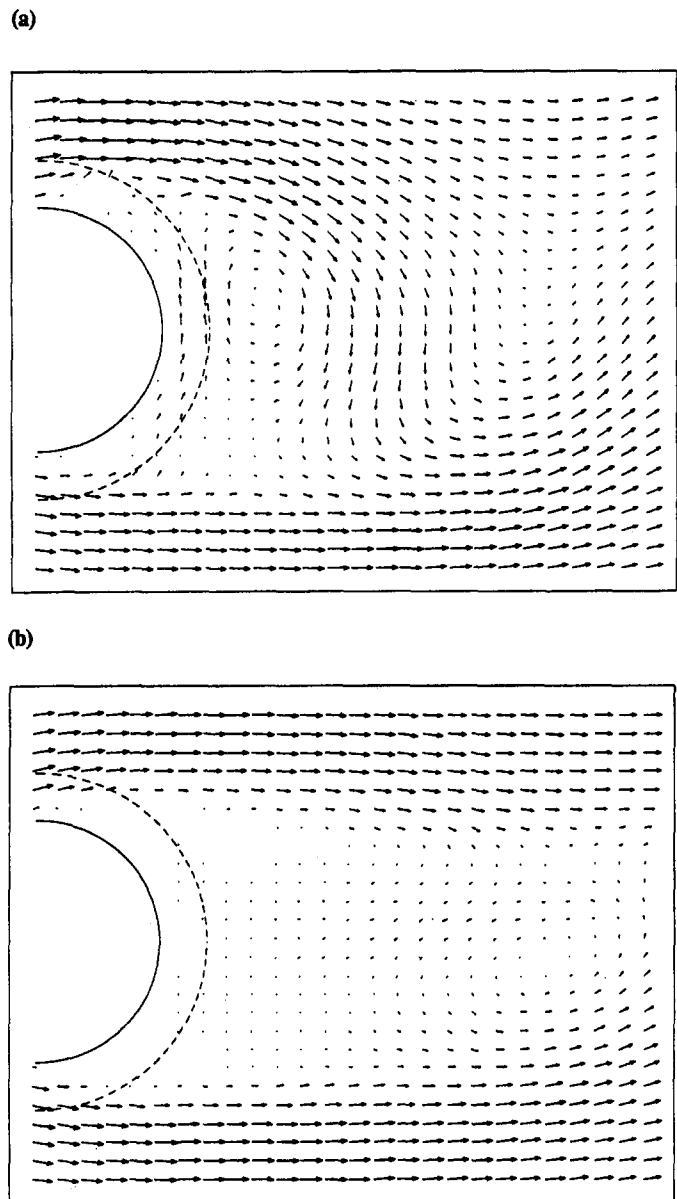


FIG. 12. Computational Velocity Vector Fields of Island 4: (a) Depth-Averaged Model; (b) Surface Velocities from 3D Model

along the wake centerline with instabilities developing in the far wake. The surface vector plot from the 3D model is shown in Fig. 12(b). Although a weak form of vortex shedding still exists in the wake, the vigor of the oscillation has reduced when compared with the 2D model run. Although the 3D model produces a more periodic and organized wake system than the laboratory flows, velocity magnitudes are approximately the same.

CONCLUSIONS

A series of laboratory experiments has been conducted to investigate the shallow recirculating flow in the wake of conical model islands with gently sloping sides. Velocity measurements using a whole-field PTV system provided benchmark data for comparison with 2D and 3D finite-difference shallow-water models.

For small values of the wake stability parameter ($S < 0.20$) the island wakes were characterized by well-organized vortex shedding systems. The effect of the angle of the island side slope on the wakes produced was found to be small. For the models tested, with slope angles ranging from 8.0 to 33.1°, the basic mechanism generating the wake was found to be the same. The 2D finite-difference model produced reasonably good predictions of the gross wake features. The assumption of hydrostatic pressure in the 3D model was considered to have a significant impact on the quality of the simulations. For flows where vertical mixing produced by the depth-varying bathymetry was an important feature, 3D models produced poorer representations of the flow field than 2D models (for which vertical mixing may be considered instantaneous). Clearly, there is need for further research in this field. Model studies without the assumption of hydrostatic pressure and with more sophisticated turbulence models are desirable.

Bed friction can act to suppress the development of vortex shedding in the wakes of conical islands. For $0.35 < S < 0.40$ an unsteady bubble-type flow was found to form in the wake of islands with side slope of 8.0 and 12.6°. This is consistent with previous results for circular islands with vertical sides. The sloping island sides thus appeared to have little effect on the transition from vortex shedding to an unsteady bubble. Flows for which the bed friction was relatively large ($S > 0.30$) were better simulated by the 3D model than by the 2D model. When modeling these flows it would appear important to represent the velocity variation across the depth. However, it is not possible to draw definitive conclusions about 2D and 3D (hydrostatic) modeling except to say that both clearly have limitations. It is maybe surprising that the 3D model does not always give better simulations.

ACKNOWLEDGMENT

This project was undertaken when Peter Lloyd was in receipt of an Engineering and Physical Sciences Research Council (EPSRC) Marine Technology studentship and we acknowledge this gratefully.

APPENDIX I. REFERENCES

- Babarutsi, S., Ganoulis, J., and Chu, V. H. (1989). "Experimental investigation of shallow recirculating flows." *J. Hydr. Engrg.*, ASCE, 115(7), 906–924.
- Berger, E., and Wille, R. (1972). "Periodic flow phenomena." *Annu. Rev. Fluid Mech.*, 4, 313–340.
- Carter, R. W., Einstein, H. A., Hinds, J., Powell, R. W., and Silberman, E. (1963). "Friction factors in open channels." *J. Hydr. Div.*, ASCE, 89(2), 97–143.
- Casulli, V. (1990). "Semi-implicit finite difference methods for the two-dimensional shallow water equations." *J. Computational Phys.*, 86(1), 56–74.
- Casulli, V., and Cheng, R. T. (1992). "Semi-implicit finite difference

- methods for three-dimensional shallow-water flow." *Int. J. Numer. Methods in Fluids*, 15(6), 629–648.
- Chen, D., and Jirka, G. H. (1991). "Pollutant mixing in wake flows behind islands in shallow water." *Environmental hydraulics*. Lee and Cheung, eds., Balkema, 371–377.
- Chen, D., and Jirka, G. H. (1995). "Experimental study of plane turbulent wakes in shallow water." *Fluid Dyn. Res.*, 16, 11–41.
- Chu, V. H., Wu, J.-H., and Khayat, R. E. (1983). "Stability of turbulent shear flows in shallow channel." *Proc., 20th Congr. of IAHR*, Moscow, U.S.S.R., 3, 128–133.
- Falconer, R. A. (1993). "Application of numerical models for water quality studies." *Proc., Instn. Civ. Engrs. Civ. Engrg.*, 93(4), 163–170.
- Falconer, R. A., Wolanski, E., and Mardapitta-Hadjipandeli, L. (1986). "Modelling tidal circulation in an island's wake." *J. Watrwy., Port, Coast., and Oc. Engrg.*, ASCE, 112(2), 234–254.
- French, R. H. (1994). *Open-channel hydraulics*. McGraw-Hill, Inc., New York, N.Y.
- Gerrard, J. H. (1966). "The mechanics of the formation region of vortices behind bluff bodies." *J. Fluid Mech.*, Cambridge, U.K., 25(2), 401–413.
- Gerrard, J. H. (1978). "The wake of cylindrical bluff bodies at low Reynolds number." *Phil. Trans. Royal Soc., Sec. A*, London, U.K., 288, 351–382.
- Hartnett, M. (1993). "Water quality aspects of offshore fish farming." *Proc. Instn. Civ. Engrs. Wat. Marit. and Energy*, 101(4), 223–235.
- Ingram, R. G., and Chu, V. H. (1987). "Flow around islands in Rupert Bay: an investigation of the bottom friction effect." *J. Geophys. Res.*, 92(C13), 14521–14533.
- Johns, B. (1991). "The modelling of the free surface flow of water over topography." *Coast. Engrg.*, 15, 257–278.
- Johns, B., Soulsby, R. L., and Xing, J. (1993). "A comparison of numerical model experiments of free surface flow over topography with flume and field observations." *J. Hydr. Res.*, Delft, The Netherlands, 31(2), 215–228.
- Johns, B., and Xing, J. (1993). "Three-dimensional modelling of the free surface turbulent flow of water over a bedform." *Continental Shelf Res.*, 13(7), 705–721.
- Lloyd, P. M. (1995). "Unsteady shallow-water wake flows." PhD thesis, University of Manchester, Manchester, U.K.
- Lloyd, P. M., Stansby, P. K., and Ball, D. J. (1995). "Unsteady surface velocity field measurement using particle tracking velocimetry." *J. Hydr. Res.*, Delft, The Netherlands, 33(4), 519–534.
- Pattiaratchi, C., James, A., and Collins, M. (1986). "Island wakes and headland eddies: a comparison between remotely sensed data and laboratory experiments." *J. Geophys. Res.*, 92(C1), 783–794.
- Stansby, P. K., and Lloyd, P. M. (1995). "A semi-implicit Lagrangian scheme for 3-D shallow water flow with a two-layer turbulence model." *Int. J. Numer. Methods in Fluids*, 20(2), 115–133.
- Wolanski, E. (1986). "Water circulation in a topographically complex environment." Lecture notes on coastal and estuarine studies, *Physics of Shallow Estuaries and Bays*, Vol. 16, J. van de Kreeke, ed., 154–167.
- Wolanski, E., Imberger, J., and Heron, M. L. (1984). "Island wakes in shallow coastal waters." *J. Geophys. Res.*, 89(C6), 10553–10569.
- Wu, J., and Tsanis, I. K. (1994). "Pollutant transport and residence time in a distorted scale model and a numerical model." *J. Hydr. Res.*, Delft, The Netherlands, 32(4), 583–598.

APPENDIX II. NOTATION

The following symbols are used in this paper:

- c_f = bed-friction coefficient;
 c_H = horizontal mixing coefficient;
 D = model island diameter;
 D_a = island diameter at middepth;
 g = gravitational acceleration;
 h = water depth;
 h_i = island height;
 k_s = bed roughness height;
 n = Manning roughness coefficient;
 R = Reynolds number;
 R_h = Reynolds number based on water depth;
 R_* = Reynolds number based on roughness parameter;
 S = wake stability parameter;

S_{c1}, S_{c2} = critical wake stability parameters;
 T_f = flushing time;
 u, v, w = orthogonal x, y, z velocity components;
 U_0 = mean free-stream velocity;
 u_* = friction velocity;

x, y, z = orthogonal coordinates;
 μ_H = horizontal eddy viscosity;
 θ = island side slope angle;
 ν = kinematic viscosity; and
 ω = z -component vorticity.